Molecular BioSystems

Accepted Manuscript

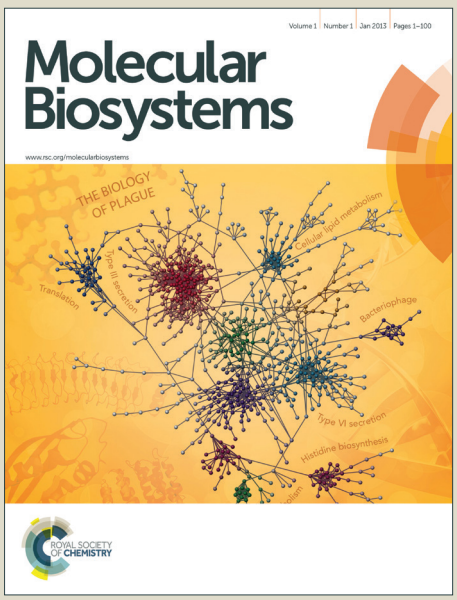

This is an *Accepted Manuscript*, which has been through the Royal Society of Chemistry peer review process and has been accepted for publication.

Accepted Manuscripts are published online shortly after acceptance, before technical editing, formatting and proof reading. Using this free service, authors can make their results available to the community, in citable form, before we publish the edited article. We will replace this *Accepted Manuscript* with the edited and formatted *Advance Article* as soon as it is available.

You can find more information about *Accepted Manuscripts* in the Information for Authors.

Please note that technical editing may introduce minor changes to the text and/or graphics, which may alter content. The journal's standard Terms & Conditions and the Ethical guidelines still apply. In no event shall the Royal Society of Chemistry be held responsible for any errors or omissions in this *Accepted Manuscript* or any consequences arising from the use of any information it contains.

ROYAL SOCIETY OF CHEMISTRY

www.rsc.org/molecularbiosystems

Cite this: DOI: 10.1039/c0xx00000x

www.rsc.org/xxxxxx

PAPER

1Modeling mitotic regulatory network identifies highly efficient anti-cancer drug combinations†

Yiran Wu,[a,b] Xiaolong Zhuo,[c] Ziwei Dai,[b] Xiao Guo,[c] Yao Wang,[c] Chuanmao Zhang*[c] and Luhua Lai*[a,b]

Received (in XXX, XXX) Xth XXXXXXXXX 20XX, Accepted Xth XXXXXXXXX 20XX

DOI: 10.1039/b000000x

Targeting mitotic regulation is recognized as an important strategy for cancer therapy. Aurora A/B kinase and polo-like kinase 1 (PLK1) are key mitotic regulators, and many inhibitors have been developed. Combinations of these inhibitors are anticipated to be more effective therapeutics compared with single-inhibitor treatments; however, a systematic analysis of the combined effects is lacking. Here, we constructed the first mammalian cell mitotic regulation network model, which spans from mitotic entry to anaphase initiation, and contains all key mitotic kinase targets. The combined effects of different kinase inhibitors and microtubule inhibitors were systematically explored. Simultaneous inhibition of Aurora B and PLK1 strongly induces polyploidy. Microtubule inhibitor dosage can be significantly reduced when combined with PLK1 inhibitor. The efficacy of these inhibitor combinations was validated by our experimental results. The mitotic regulatory network model provides a platform to study complex interactions during mitosis, enables identification of mitotic regulators, and determines targets for drug discovery research. The suggested use of combining microtubule inhibitors with PLK1 inhibitors is anticipated to enhance microtubule-inhibitor tolerance in a wide range of patients.

Introduction

Eukaryotic cell division occurs during mitosis. To ensure that two identical copies of DNA are distributed to the two daughter cells, mitosis is tightly controlled. Mitotic failure results in genomic instability, which may cause cell death or cancer.[1-3] Cell proliferation is more active in cancer cells compared with normal cells; therefore, strategies to disrupt mitosis are utilized for anti-cancer therapy.[4] Microtubule inhibitors, which block microtubule dynamics and cause abnormal mitotic spindles, are successfully used in clinical applications. However, these agents have adverse side effects, such as peripheral neuropathy, because microtubules have important functions in non-mitotic cells.[5, 6] Research on mitotic regulatory mechanisms has provided insight into this complex process. Several proteins with unique functions in mitosis were identified as novel anti-cancer drug targets, such as mitotic kinases, kinesins, and checkpoint proteins.[7]

Aurora kinases and polo-like kinase 1 are mitotic kinases that have attracted much attention. Human Aurora kinases are classified as three types designated as Aurora A, Aurora B, and Aurora C. Aurora A is required for centrosome maturation and spindle assembly, and participates in activation of cyclin-dependent kinase 1 (CDK1), the key kinase that controls progression of mitosis during mitotic entry. Aurora B is a component of the chromosome passenger complex and regulates chromatid separation by destabilizing incorrect kinetochore-microtubule attachment. Expression of Aurora C is limited to the testes, and it functions only during meiosis. Aurora A/B were overexpressed in several cancer cell lines, and are considered as potential anti-cancer drug targets.[8, 9] Pan-Aurora kinase inhibitors and selective inhibitors of Aurora A/B are currently under development, although the benefit of Aurora isoform specificity is unclear.[10-12] Polo-like kinase 1 (PLK1) is the most investigated protein of the polo-like kinase family, which has five members. PLK1 has multiple functions in cell-cycle control. During mitosis, it regulates mitotic entry, centrosome biogenesis, mitotic chromosomes, and cytokinesis. PLK1 overexpression is linked with cancer, and it is identified as a promising drug target.[13, 14] Several PLK1 inhibitors have been developed, and some are under clinical or preclinical study. In 2013, volasertib (BI 6727, for treating acute myeloid leukemia) became the first PLK1 inhibitor received the FDA's new "Breakthrough Therapy" designation and is under consideration for accelerated approval.[15] Considering the functions of these kinases and the phenotypes induced by their inhibitors, combination therapy using Aurora or PLK1 inhibitors is anticipated to be highly effective.[16] However, systematic

† Electronic supplementary information (ESI) available: Table S1–S3, Fig. S1–S3. See DOI: 10.1039/b000000x/

[a] BNLMS, State Key Laboratory for Structural Chemistry of Unstable and Stable Species, and Peking-Tsinghua Center for Life Sciences at College of Chemistry and Molecular Engineering, [b] Center for Quantitative Biology, [c] The Ministry of Education Key Laboratory of Cell Proliferation and Differentiation and the State Key Laboratory of Biomembrane and Membrane Biotechnology, College of Life Sciences, Peking University, Beijing 100871, China.

* Corresponding authors. C Zhang, Tel.: +86 10 6275 7173; Fax: +86 10 6276 7246; E-mail: zhangcm@pku.edu.cn or L Lai, Tel.: +86 10 6275 7486; Fax: +86 10 6275 1725; E-mail: lhlai@pku.edu.cn

Molecular BioSystems Accepted Manuscript

experimental and theoretical investigations are lacking.

Constructing and simulating biological networks is widely used in cell-cycle studies, and mitosis has been modeled at different levels. Tyson and Novák generated network models describing CDK1 regulation, and integrated the module into whole cell-cycle models.[17-20] Ferrell et al. modeled CDK1 regulation in *Xenopus* oocytes using two positive-feedback loops (Wee1 and CDC25) and one negative-feedback loop (anaphase promoting complex/cyclosome, APC/C), and obtained the oscillation dynamics predicted from experiments.[21-25] Several network models of spindle-assembly checkpoint were published, including biophysical and molecular models (for review see Ref. [26]). The first model of mitotic entry containing Aurora A and PLK1 was reported by Zou et al. in 2011.[27] Aurora kinases and PLK1 play important roles in both mitotic entry and spindle-assembly checkpoint, but no quantitative discussion has been published. Therefore, a more comprehensive network model simulating multiple mitotic phases is required to test the therapeutic effects of Aurora and PLK1 inhibitor combinations, and to identify potential nodes for new drug targeting.

We constructed a model for the whole mitotic regulatory network that describes mitosis from prophase to anaphase. The model contains all three potential kinase targets, including Aurora A/B and PLK1, and can be used to analyze the anti-cancer effects of drug regimens. Dynamic simulation of the network model enabled prediction of several potent dual-target combinations, and these predictions were validated by performing experimental studies.

Results

Mitotic Regulatory Network

We constructed a theoretical model of the mitotic regulatory network to simulate the progression through mitosis (Fig. 1). The network model contains the following four modules, and each module has an output species: (1) regulation of CDK1 activity (CDK1:CycB); (2) inter-regulation between Aurora A and PLK1, which promotes centrosome maturation and spindle formation [centrosomal p-AurkA (p-AurkA-cs)]; (3) kinetochore-microtubule attachment (Attached); and (4) spindle-assembly checkpoint (APC/C:CDC20). This network was generated using information retrieved from experimental reports, review articles, and published network models of mitotic stages (see subsequent discussion).

CDK1 is the key enzyme in mitosis. In our network model, CDK1 is activated by dephosphorylation of Tyr15 during entry to mitosis, and inactivated by degradation of the Cyclin B activator after spindle-assembly checkpoint is turned off. The effects of Wee1 and CDC25 are described in published models.[18-22, 27] CDK1 binding to Cyclin B is not considered in our model because Cyclin B level reaches maximum before the initial time point of our model.[28]

Aurora A and PLK1 have important roles in mitotic entry and spindle formation.[16] The Aurora A/Bora/PLK1 pathway in our

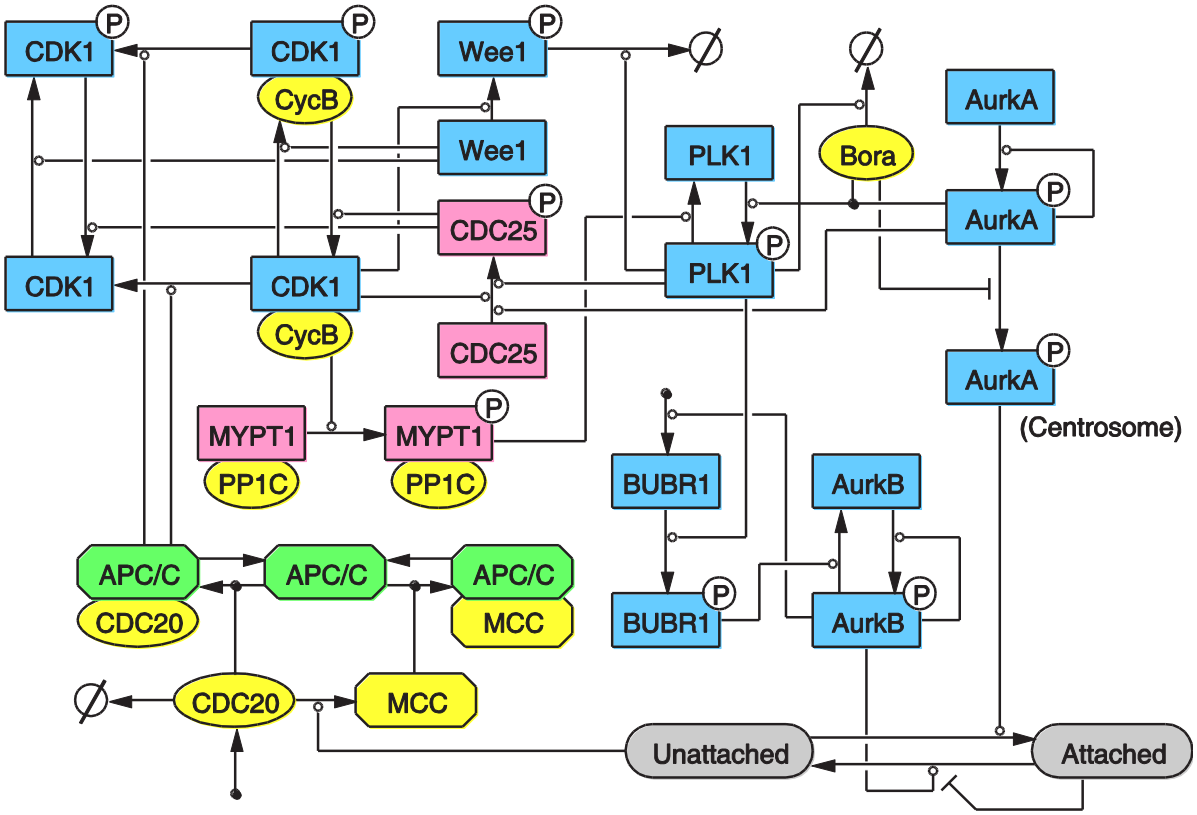

Fig. 1 Mitotic regulatory network. The network contains four modules: (1) CDK1 regulation, top left; (2) inter-regulation between Aurora A and PLK1, top right; (3) kinetochore-microtubule attachment, bottom right; and (4) spindle-assembly checkpoint, bottom left. Species functions are denoted by color: kinase (blue), phosphatase (pink), ubiquitin ligase (green), non-enzymatic protein/complex (yellow), and attachment states (gray)

Molecular BioSystems Accepted Manuscript

model is based on a report that Bora and Aurora A cooperatively activate PLK1.[28] Previous work also based this pathway on the same report.[27] Localization of Aurora A on centrosome is regulated by PLK1 by triggering the degradation of Bora.[29]

Kinetochore-microtubule attachment is a complex stochastic process. Before microtubules from opposite spindle poles attach to sister kinetochores (amphitelic orientation), single attachment (monotelic orientation) is an obligatory step. Misattachments (syntelic and merotelic orientations) may occur. Merotelic orientation is related to the thickness of attachment bundles from different spindle poles.[30] This process cannot be accurately described in detail in the mitotic regulatory network. We constructed a two-state description of kinetochore-microtubule attachment and define the states as unattached and attached. Aurora A promotes the transition from unattached to attached, whereas Aurora B destabilizes the attachment and promotes transition from attached to unattached. The transition time is used to indicate mitotic delay and chromosome instability. This description is similar to the biological model developed by Mistry et al.[31]

Spindle-assembly checkpoint prevents anaphase onset until all chromosomes are correctly attached to the mitotic spindle. This pathway inhibits the function of CDC20, a co-factor of E3 ubiquitin ligase anaphase-promoting complex/cyclosome (APC/C). Mitotic-checkpoint complex (MCC), which contains CDC20, is the spindle-assembly checkpoint effector.[32] Network models of MCC formation have been constructed to simulate mitotic dynamics.[33-37] MCC formation in our model is simplified to one reaction: transition from CDC20 to MCC. Synthesis and degradation of CDC20 are included in our network model, for these reactions determined the CDC20 level.[38-41]

Mitotic regulatory network dynamics are formulated in ordinary differential equations (ODEs). The computational model contains 27 equations that describe 29 reactions. Of these, 21 are enzymatic reactions with Michaelis-Menten kinetics, and the remaining 8 are protein-protein binding/dissociation reactions with mass-action law kinetics. The equations are presented in Table S1. Molecular concentrations were specified according to published reports. The proportions of molecules in different phosphorylation or protein-binding states at the initial time point were set as parameters (see Table S2 for details).

Parameter Optimization

The computational model contained 44 kinetic parameters and 11 initial concentration parameters. All parameters were obtained by fitting to the following published experimental data: (1) one curve from a fluorescence resonance energy transfer (FRET) experiment on CDK1 activity;[42] (2) five sets of western blot data measuring the concentrations of different molecular species (only the points from 9 to 12 hours after G1/S transit were chosen).[28, 43] All experiments were conducted using HeLa cells. Parameter fitting was performed using a method developed by our group called differential simulated annealing (DSA).[44] Parameter perturbation was used to select parameter sets that the ODE solver processes until a stable state is reached. Calculations for parameter optimization are described in Materials and Methods.

A total of 137 parameter sets were obtained from 1,000 independent simulations (see Fig. S1 for the distribution range of each parameter). Using these parameter sets, computed curves are consistent with experimental data (Fig. 2). For other molecular species not used in curve fitting, the kinetics meets known fact in mitosis (Fig. S2). The computational model using all 137 parameter sets reproduces the behavior of mitosis.

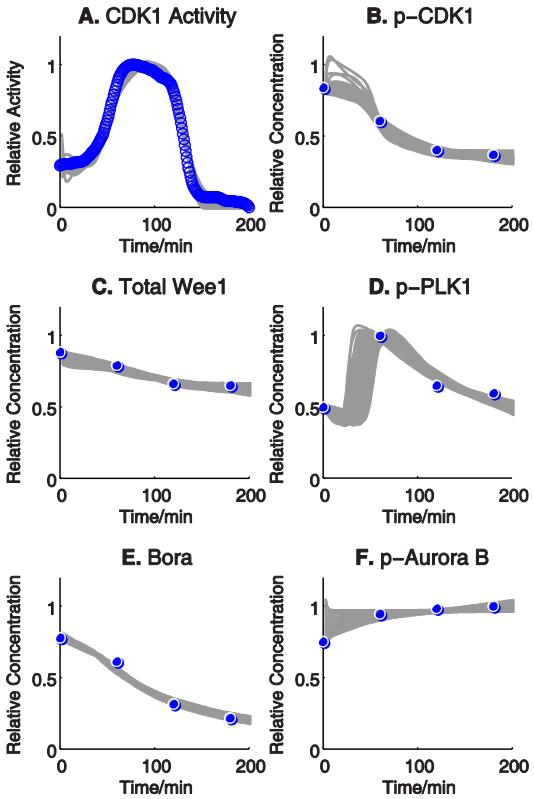

Fig. 2 Parameter-fitting for the mitotic regulatory network. Gray lines represent simulated curves of 137 parameter sets. Blue circles represent published data for molecular species concentration from: (A) FRET experiments;[42] (B−F) western blot experiments.[28, 43]

Parameter Sensitivity Analysis Identifies Key Network Regulators

To identify key reactions that affect network dynamics, single-parameter sensitivity analysis was performed. The effect of each reaction on the dynamics of the four output species (corresponding to the four modules) was calculated and ranked (see Materials and Methods section). The 10 most sensitive reactions were identified as key reactions for each output species (Table 1).

Many of the top-ranked reactions are catalyzed by Aurora kinases and PLK1, which are known key regulators of mitosis. Aurora A autoactivation and its activation of PLK1 are crucial for centrosome maturation (p-AurkA-cs) and kinetochore-microtubule attachment (Attached). Aurora B autoactivation and its inhibition of attachment are crucial for kinetochore-microtubule attachment and spindle-assembly checkpoint signal (APC:CDC20). The two reactions in which PLK1 regulates Aurora A localization (PLK1 promotes Bora degradation and Bora inhibits AurkA localization) greatly affect centrosome maturation. These results are consistent with the functions of Aurora kinases and PLK1.

Molecular BioSystems Accepted Manuscript

Table 1. Most sensitive key reactions for each output species

Rank	p-AurkA-cs	Attached	APC/C:CDC20	CDK1:CycB
1	Bora inhibits AurkA localization	AurkA autoactivation	CDC20 degradation	CDC25 activates CDK1
2	PLK1 promotes Bora degradation	AurkB autoactivation	CDC20 synthesis	APC promotes CycB degradation
3	AurkA autoactivation	AurkA promotes kinetochore -microtubule attachment	BUBR1 promotes AurkB dephosphorylation	CDC20 degradation
4	AurkA activates PLK1	Bora inhibits AurkA localization	CDC20 forms MCC	CDC20 synthesis
5	MYPT1 inhibits PLK1	BUBR1 promotes AurkB dephosphorylation	AurkB autoactivation	Wee1 inhibits CDK1
6	CDK1 activates MYPT1	AurkB inhibits kinetochore -microtubule attachment	AurkA promotes kinetochore -microtubule attachment	CDC20 forms MCC
7	CDC25 activates CDK1	PLK1 promotes Bora degradation	Bora inhibits AurkA localization	AurkA autoactivation
8	APC promotes CycB degradation	MYPT1 inhibits PLK1	AurkB inhibits kinetochore -microtubule attachment	BUBR1 promotes AurkB dephosphorylation
9	Wee1 inhibits CDK1	PLK1 recruits BUBR1	APC binds CDC20	APC binds CDC20
10	CDC20 degradation	AurkA activates PLK1	PLK1 promotes Bora degradation	AurkB autoactivation

Most of the top-ranked reactions have been reported to affect mitotic regulation. Our parameter-sensitivity analysis indicates that the reaction BUBR1 promotes AurkB dephosphorylation largely affects both kinetochore-microtubule attachment and APC/C:CDC20 activity. This is consistent with published reports that BUBR1 regulates spindle-assembly checkpoint and inhibits APC/C:CDC20 activity.[45, 46] CDC20 synthesis is crucial for spindle-assembly checkpoint and CDK1 activity. Kidokoro et al. reported that CDC20 expression was suppressed by p53, and identified CDC20 as an anti-cancer target.[47] Cyclin B degradation ranks high for spindle-assembly checkpoint and CDK1 activity. The E2 ubiquitin-conjugating enzyme of this degradation pathway, UbcH10, was closely implicated in cancer.[48, 49] These results validate our computational simulations, and demonstrate that our model can predict the effects of targeted disruption of mitosis.

Network Simulation Validates Aurora A/B as a Beneficial Therapeutic Target

Many inhibitors have been developed to target Aurora A/B since they were identified as potential anti-cancer drug targets. Approximately 30 compounds are in clinical or pre-clinical development, including pan-Aurora kinase inhibitors and selective inhibitors of Aurora A or Aurora B.[10] However, the effect of combination targeting of Aurora A/B has not been evaluated at a biological or network level. Although pan-Aurora kinase inhibitors cause mitotic-spindle defects that are consistent with Aurora A inhibition, the resultant phenotype is polyploid (typical for Aurora B inhibition) rather than mitotic blockade (typical for Aurora A inhibition).[50-52] This bypass of Aurora A by Aurora B inhibition is supported by RNAi experiments, but the molecular mechanism is unknown.[53] We used our network model to simulate the effects of combined inhibition of Aurora A/B.

Aurora A inhibition was expressed as the rate reduction of all reactions catalyzed by Aurora A after non-competitive inhibition.

$$\frac{d[S]}{dt} = -\frac{k_{cat}[E][S]}{(K_M + [S])\left(1 + \frac{[I]}{K_i}\right)}$$

$[I]$ is concentration of the inhibitor and K_i is the inhibitory constant. The doses were set to $\log_{10}\frac{[I]}{K_i}$ every 0.25 from −1 to 1. Aurora B inhibition was expressed in the same way. Effects of combined inhibition at each dosage pair were calculated. Simulated curves of phosphorylated Aurora A at centrosome and kinetochore-microtubule attachment are presented in Fig. 3. For clarity, only selected dose results are presented. For Aurora A, $\log_{10}\frac{[I]}{K_i} = 0$ (50% inhibition) or $\log_{10}\frac{[I]}{K_i} = 0.5$ (76% inhibition).

Molecular BioSystems Accepted Manuscript

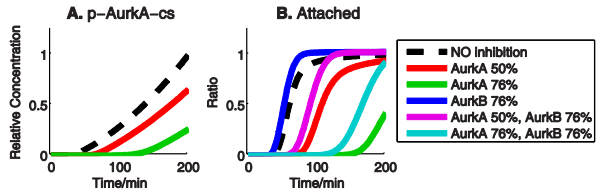

Fig. 3 Simulations for combined inhibition of Aurora A/B. (A) Centrosome maturation represented by phosphorylated Aurora A at the centrosome (normalized to the value at 200 min with no inhibition). (B) Kinetochore-microtubule attachment represented by the ratio of attached kinetochore.

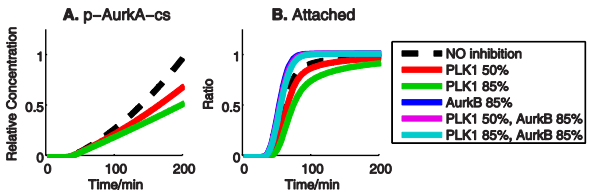

Fig. 4 Simulations from combined inhibition of Aurora B and PLK1. The representations are the same as in Fig. 3.

For Aurora B, $\log_{10}\frac{[I]}{K_i}$ = 0.5 (76% inhibition). Each of the 137 parameter sets was used in the calculation; only the parameter set nearest to the centroid of the parameter-distribution was presented as a representative simulation result (the centroid is defined as the point having the least total distance to all the parameter sets in the parameter space with logarithmic coordinates; cityblock distances are used). Results of other parameter sets are similar with the one shown here. The same constraints apply for all subsequent analyses.

Aurora A inhibition delays centrosome maturation and kinetochore-microtubule attachment in the mitotic network model. This is consistent with experimental results showing that Aurora A inhibition delays mitosis. Aurora B inhibition does not affect centrosome maturation but enables kinetochore-microtubule attachment at an earlier time point. Aurora B inhibition leads to formation of the kinetochore-microtubule attachment before mature centrosomes are generated, turns off the spindle-assembly checkpoint, and results in polyploidy. The kinetochore-microtubule attachment time shift due to Aurora B inhibition increases with the Aurora A inhibitor dosage. This result indicates that combined inhibition of Aurora A/B more potently induces polyploidy. This is consistent with published experimental data using knockdowns; inactivation of both Aurora A/B generates more polyploid cells than inactivation of only Aurora B.[53]

Combined Inhibition of Aurora B and PLK1 Effectively Generates Polyploidy

Aurora A and PLK1 are both required for spindle assembly; therefore, combined inhibition of Aurora B and PLK1 may have similar effects as combined inhibition of Aurora A/B. We simulated the effect of combined inhibition of Aurora B and PLK1 to test this hypothesis using the same computational methods that were used for testing Aurora A/B inhibition. Simulation results are presented in Fig. 4. For clarity, only selected dose results are presented. For PLK1, $\log_{10}\frac{[I]}{K_i}$ = 0 (50% inhibition) and $\log_{10}\frac{[I]}{K_i}$ = 0.75 (85% inhibition). For Aurora B, $\log_{10}\frac{[I]}{K_i}$ = 0.75 (85% inhibition).

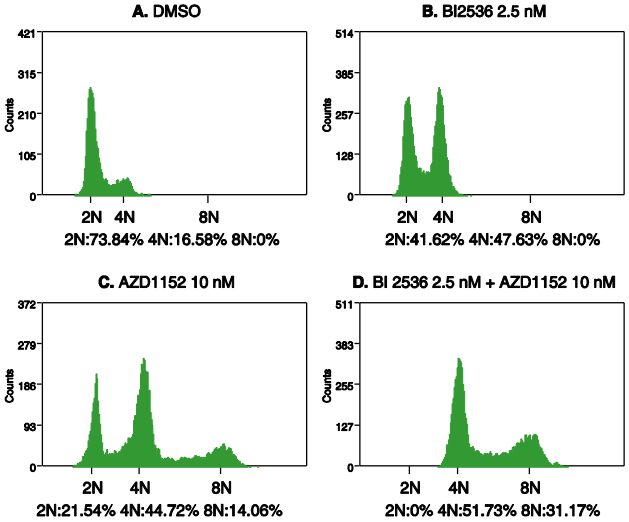

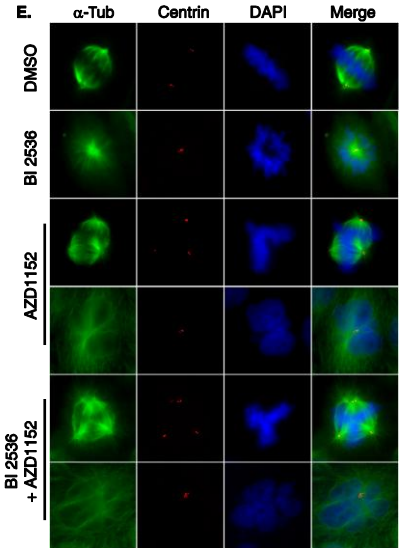

Fig. 5 Experimental effects of combined PLK1 and Aurora B inhibitors on HeLa cells. (A–D) HeLa cell DNA contents were measured using flow cytometry. Cells were treated with (*A*) DMSO, (B) BI 2536, (C) AZD1152, or (D) BI 2536 and AZD1152. (E) Immunostaining of α-tubulin (α-Tub) and Centrin in HeLa cells; cells were treated with DMSO, BI 2536, AZD1152, or BI 2536 and AZD1152. Scale bar=10 μm.

Inhibition of PLK1 delays centrosome maturation and kinetochore-microtubule attachment, similar to the effects of Aurora A inhibition, but the kinetics are different. PLK1 indirectly regulates Aurora A, in that PLK1 controls Aurora A localization by promoting Bora degradation.[29] For this reason, combined inhibition of PLK1 and Aurora B generates similar results as that of singly inhibiting Aurora B. The time shift for inhibition is lengthened with simultaneous inhibition of PLK1 and Aurora B. Therefore, combined inhibition of PLK1 and Aurora B more effectively produces polyploidy. We experimentally tested the combined inhibition of PLK1 and

Molecular BioSystems Accepted Manuscript

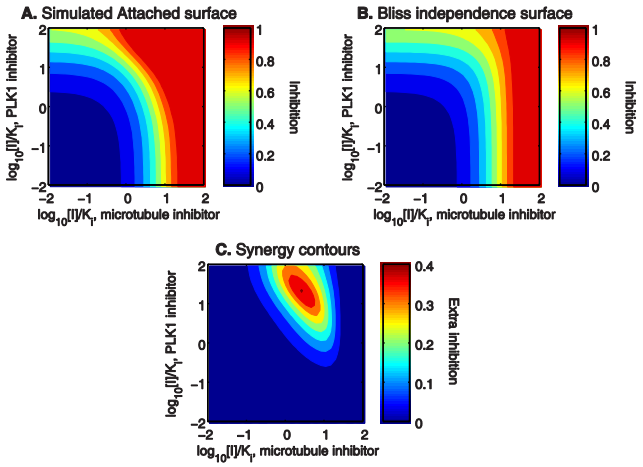

Fig. 6 Response surface of microtubule inhibitor and PLK1 inhibitor for kinetochore-microtubule attachment. (A) Simulated surface; (B) Bliss independent surface; (C) synergy contours are the difference between simulated surface and Bliss independence surface.

Aurora B. HeLa cells were treated with the PLK1 inhibitor BI 2536 (2.5 nM) and the selective Aurora B inhibitor AZD1152 (10 nM) individually or combined for 24 h. Cell DNA contents were measured using flow cytometry (Fig. 5). As expected, PLK1 inhibitor causes mitotic arrest, whereas Aurora B inhibitor causes polyploidy (14.06% of cells with DNA content 8*N*). Cells treated with both PLK1 and Aurora B inhibitors exhibited significantly higher index of polyploidy (31.17%). This result is in agreement with our mitotic network simulation, and indicates that inhibition of PLK1 and Aurora B is a potent anti-cancer drug-target combination.

Effective Microtubule Inhibitor Dosage Is Reduced by Combination with PLK1 Inhibitor

Microtubule inhibitors are a class of drugs that target mitosis, and are successfully used in cancer therapy. However, these drugs have adverse side effects including neurotoxicity and myelosuppression, because microtubules have important functions in normal cells. Combination therapies using microtubule inhibitors with other drugs may improve drug efficacy and reduce adverse side effects.[5] The advantage of combining microtubule inhibitors with mitotic kinase inhibitors has been postulated previously,[16] but a systematic study has not been reported. Network simulation is an efficient method to identify synergistic drug combinations.[54, 55] Using our network model, we studied the combined effects of microtubule inhibitors with Aurora A/B or PLK1 inhibitors on kinetochore-microtubule attachment.

Microtubule assembly inhibition was modeled as a rate decrease in the transition from unattached to attached kinetochores. Inhibition of Aurora kinases or PLK1 was expressed as described previously. The doses were set to $\log_{10}\frac{[I]}{K_i}$ every 0.125 from −2 to 2. Inhibitor response was represented by the area under the curve of attached kinetochores. Synergy was quantified using the Bliss independence model, which assumes that inhibitors act through distinct mechanisms.[54] The response surfaces were generated using 1,089 dose pairs.

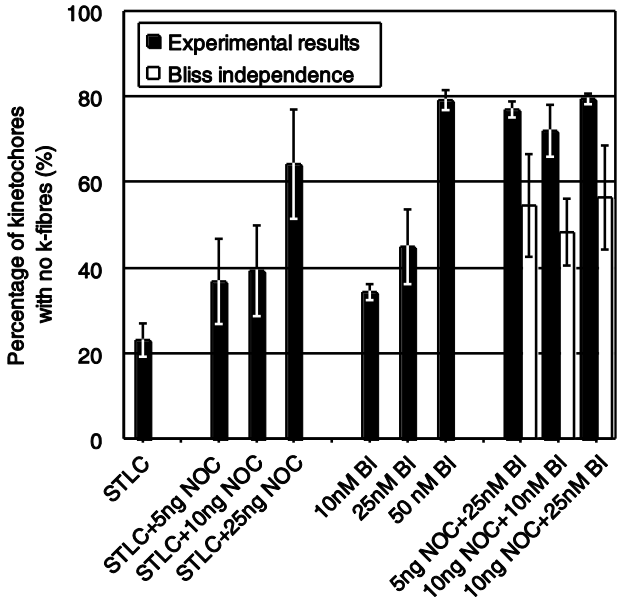

Fig. 7 Quantification of kinetochore-microtubule attachment (black) for HeLa cells treated with microtubule inhibitor nocodazole (NOC) and/or PLK1 inhibitor BI 2536 (BI), with *S*-trityl-L-cysteine (STLC) as negative control for BI 2536. Each data point represents three independent experiments; error bars indicate standard error. For combined inhibition, Bliss independence percentages (white) are shown.

We tested inhibitors of Aurora A/B kinases and PLK1; only PLK1 inhibitor was significantly synergistic with microtubule inhibitor (Fig. 6). The maximum additional inhibition reaches 40% near the dosage close to the K_i value of microtubule inhibitor. The four reactions catalyzed by PLK1 (promote p-Wee1 degradation, CDC25 phosphorylation, promote Bora degradation, and recruit BUBR1) were simulated separately to test the effect of combining PLK1 inhibitor with microtubule inhibitor. The results show that the synergistic effect is primarily due to the reaction recruit BUBR1, which regulates kinetochore-microtubule attachment through an alternative pathway that does not depend on microtubule formation. Parallel pathways represent a common network architecture for drug synergy.[56]

The simulation results indicate that microtubule inhibitor effect is enhanced by a PLK1 inhibitor, and will achieve a better effect at a lower microtubule inhibitor dose. We designed an experiment to quantitatively measure the synergy effect by using different concentrations of microtubule inhibitor and/or PLK1 inhibitor to treat cells, and quantifying the percentage of unattached kinetochores. This experiment was performed using HeLa cells. Nocodazole was the microtubule inhibitor, and BI 2536 was the PLK1 inhibitor. To induce mono-astral spindles similar to that of PLK1 inhibition, 5 nM *S*-trityl-L-cysteine (STLC) was used in addition to nocodazole; treating cells with STLC alone served as negative control. For each concentration pair of nocodazole and BI 2536, the Bliss independence percentage of unattached kinetochores was calculated.

For either nocodazole or BI 2536, three concentration values were used to generate partial inhibition of kinetochore-microtubule attachment. Then, three concentration pairs with

Molecular BioSystems Accepted Manuscript

middle or low concentration of both inhibitors were tested for synergistic effects. At each concentration pair, the effect of nocodazole and BI 2536 combined is approximately 20% higher than the Bliss independence value (Fig. 7). For all three concentration pairs, the ratio of unattached kinetochores exceeds the value obtained when using 25 ng nocodazole alone. Combination of 10 ng nocodazole and 25 nM BI 2536 achieves approximately 80% unattached kinetochores. This experimental result validates our simulation prediction that simultaneously using microtubule inhibitor and PLK1 is a potent anti-cancer therapeutic strategy.

Discussion and Conclusions

Combination drug therapy is widely used to treat diseases due to higher effectiveness, lower dose and toxicity, and/or less resistance. Considerable effort has been invested to quantitatively measure dose-effects of drugs and drug combinations.[57] From a systems point of view, it is necessary to use biological network models of diseases to investigate all possible effects of single drugs or drug combinations. Mathematical models based on molecular reaction-rate laws provide quantitative descriptions of the system. Time-course network simulation reveals dynamic behavior, and drug actions can be modulated using system-level perturbations (for review see Ref. 58). Here we constructed a model of mitotic regulatory network with ODE. This is the first molecular level model of mitosis spanning from mitotic entry to anaphase initiation. The network model contains all key mitotic kinase targets and can be used to simulate the effects of different types of agents. Though experimental data can be used in curve fitting is not sufficient to determine a unique parameter set (the parameter distribution ranges are large, Fig. S1), the accuracy of our model is validated by successfully reproducing the dynamic behavior of the system, identifying key reactions through parameter sensitivity analysis, and predicting several efficient anti-cancer drug combinations which are validated by experiments. Using an ensemble of parameter sets has been applied in several studies in systems biology, for example, model selection[59] and metabolism modeling[60]. Our work also supports the use of network simulations with ensemble-based approach as powerful tools to identify novel therapeutic strategies for the treatment complex diseases.

Our simulation explains the published experimental result exhibiting bypass of Aurora A by Aurora B inhibition.[53] Simultaneously inhibiting Aurora A/B is validated as an effective strategy, which efficiently generates a greater number of polyploid cells compared with that of Aurora A or Aurora B inhibition. Therefore, research efforts to develop pan-Aurora kinase inhibitors and selective inhibitors of Aurora A or Aurora B are expected to provide new and beneficial therapeutic strategies. The effectiveness of different inhibitor types may depend on specific cell line properties or cancer types. Hence, extensive experimental and clinical validation of identified kinase inhibitors also will be required.

Two highly efficient anti-cancer drug combinations, Aurora B/PLK1 and microtubule formation/PLK1, were identified through simulation. The time shift due to Aurora B inhibition increases with PLK1 inhibitor dosage, therefore the effect of Aurora B inhibitors, polyploidy, will be strengthened. In our experiment, cells treated with both Aurora B and PLK1 inhibitors exhibited much higher index of polyploidy, validating the prediction of our simulation. Therefore Aurora B/PLK1 is an efficient anti-cancer drug target combination.

Simulation shows inhibiting microtubule formation and PLK1 activity is synergistic, and our experiment reveals treating cells with this inhibitor combination is highly effective at lower concentrations. Microtubule inhibitors are currently used in clinic but have adverse side effects.[5, 6] According to our prediction, combined using of PLK1 inhibitor can reduce the dosage of microtubule inhibitor. Therefore this combination may overcome the adverse side effects thus is a potent strategy for treating cancer. Of course, the effectiveness of the two anti-cancer drug combinations we proposed needs further experimental study on animal models and cancer patients.

Materials and Methods

Parameter Fitting and Sensitivity Analysis

Differential simulated annealing (DSA) is a modified simulated annealing method based on local second-order approximation. DSA has good performance in parameter fitting during complex network simulation.[44] The ODE solver used for the present study was gsl_odeiv2_msbdf in GNU Scientific Library (GSL). The objective function of the mitotic regulatory network is

$$f = \frac{1}{28}\left[\sum_i \sum_j \left(\hat{W}_i(t_j) - W_{ij}\right)^2 + \sum_i \left(\frac{\hat{F}(t_i) - F_i}{5}\right)^2\right] + \sum_i P_i^2$$

where W_{ij} is the experimental value of the ith set of western blot data at the jth time point; $\hat{W}_i(t_j)$ is the predicted value; F_i is the experimental value of the FRET data at the ith time point; and $\hat{F}(t_i)$ is the predicted value. The FRET data points were retrieved every minute from published results[42], resulting 201 points. As there are 20 Western blot data points for fitting, a weight coefficient of 5 (based on experience) is introduced to the FRET item. Penalty functions (P_i) are constraints of parameters or simulated curves. Initial concentration ratio parameters of one substance have relations, which is expressed by a penalty function. Penalty functions for curves are added to avoid unnatural kinetics for species not used for fitting. All penalty function formulas are listed in Table S3.

The initial ranges of kinetic parameters were determined to make velocities of reactions in proper magnitude. Each parameter range covers 4 magnitudes. For Michaelis-Menten equations, first k_{cat} were set to 1 to 10^4 min^{-1}, and K_M were then decided. A total of 1,000 independent simulations were run, and 421 reached convergence. Perturbation of every single parameter was performed for all 421 sets. For a kinetic parameter k, the perturbed parameter $k' = rk$ (r = 5, 25, 125, 1/5, 1/25, and 1/125); for an initial concentration proportion parameter a, the perturbed parameter $a' = \frac{ra}{1+(r-1)a}$ (r takes the same value). The formula for the initial concentration proportion parameter a is derived as follows: transformation of a (range, 0 to 1) to k (range, 0 to ∞), and thereafter $k = \frac{a}{1-a}$. For each parameter set, if solving the ODE fails in a perturbed condition, the parameter set is considered unstable and rejected. Finally, 137 parameter sets were retained.

Molecular BioSystems Accepted Manuscript

The sensitivity S of each kinetic parameter (k, because initial concentration proportion parameters were not included for sensitivity analysis) was calculated based on the result of parameter perturbation

$$S = \sum_i \sum_j \frac{\Delta A_{ij}}{w_j}$$

where ΔA_{ij} is the area between the original and jth perturbed computing curve of the ith output species; w_j is the weight for the jth perturbation, $w_j = r_j$; $r_j > 1$; and $w_j = \frac{1}{r_j}$ for $r_j < 1$. For each parameter set, the sensitivities of all kinetic parameters were ranked in descending order. Then, the median rank of each parameter in 137 parameter sets was calculated, and all median values were sorted in ascending order as a sensitivity sequence of kinetic parameters in all sets. Then, the parameter sequence was merged with the reaction sequence. For an enzymatic reaction with two parameters, the more sensitive position was taken and the other was removed.

Cell Culture and Analysis of Cell-Cycle Progression

HeLa cells (female) were seeded onto 6-well plates (3×10^4 cells/well) and cultured overnight at 37 ℃ in a 5% CO_2 atmosphere in DMEM (Gibco, Grand Island, NY) with 10% fetal bovine serum (HyClone Laboratories Inc., Logan, UT), 100 U/mL penicillin, and 100 μg/mL streptomycin (Invitrogen, Grand Island, NY). After treating with DMSO, 2.5 nM BI 2536 (Axon Medchem, Groningen, The Netherlands), or 10 nM AZD1152 (Selleck, Huston, TX) individually or in combination for 24 h, cells were detached with trypsin and collected by centrifugation at 1,000×g for 5 min. After washing twice with phosphate buffered saline (PBS), the cells were fixed in 70% ethanol-PBS for 2 h at 4 ℃, and then washed with PBS and collected by centrifugation. For analysis of cell-cycle progression, the cells were analyzed by Becton Dickinson FACScan (BD Biosciences, San Jose, CA) after treating with 400 μL PBS-containing 100 mg/mL RNase, 1% Triton X-100, and 0.5 mg/mL propidium iodide for 30 min at 37 ℃.

Immunofluorescence and Microscopy Quantifications

HeLa cells grown on glass coverslips were arrested at G1/S by treating with 2.5 mM thymidine (Sigma, St Louis, MO) for 18 h. After release into fresh medium containing STLC, different concentrations of nocodazole (Sigma, St Louis, MO) and BI 2536 were added individually or in combination for 12 h, and cells were fixed in cold methanol for 5 minutes. Coverslips were incubated overnight at 4 ℃ with anti-α-tubulin (Sigma, St Louis, MO) and anti-centromere (Antibodies Inc., Davis, CA, 15-234-0001) diluted 1:200 in PBS with 3% bovine serum albumin, washed with PBS, and incubated with fluorescently labeled secondary antibodies for 1 h at room temperature. After washing with PBS, the coverslips were mounted with Mowiol (Sigma-Aldrich, St Louis, MO) containing 1 μg/mL 4',6-diamidino-2-phenylindole (DAPI, Sigma-Aldrich, St Louis, MO) to stain DNA. Cells were analyzed with an Olympus IX-71 inverted microscope with a 60x1.42 oil objective. For quantification of kinetochore-microtubule attachment, more than 100 cells were measured for each sample.

Acknowledgments

We thank all members of the Lai and Zhang laboratories for valuable comments. This work was supported in part by grants from the Ministry of Science and Technology of China (2012AA020308, 2010CB833705) and the National Natural Science Foundation of China (NSFC) (31030044, 91313302 and 31371365).

References

1. G. J. Kops, B. A. Weaver and D. W. Cleveland, *Nat. Rev. Cancer*, 2005, **5**, 773-785.
2. Z. Storchova and D. Pellman, *Nat. Rev. Mol. Cell Biol.*, 2004, **5**, 45-54.
3. N. J. Ganem, Z. Storchova and D. Pellman, *Curr. Opin. Genet. Dev.*, 2007, **17**, 157-162.
4. E. Manchado, M. Guillamot and M. Malumbres, *Cell Death Differ.*, 2012, **19**, 369-377.
5. M. A. Jordan and L. Wilson, *Nat. Rev. Cancer*, 2004, **4**, 253-265.
6. C. Dumontet and M. A. Jordan, *Nat. Rev. Drug Discov.*, 2010, **9**, 790-803.
7. V. Sudakin and T. J. Yen, *BioDrugs*, 2007, **21**, 225-233.
8. J. Fu, M. Bian, Q. Jiang and C. Zhang, *Mol. Cancer Res.*, 2007, **5**, 1-10.
9. O. Gautschi, J. Heighway, P. C. Mack, P. R. Purnell, P. N. Lara, Jr. and D. R. Gandara, *Clin. Cancer Res.*, 2008, **14**, 1639-1648.
10. M. Kollareddy, D. Zheleva, P. Dzubak, P. S. Brahmkshatriya, M. Lepsik and M. Hajduch, *Invest. New Drugs*, 2012, **30**, 2411-2432.
11. S. Abraham, M. J. Hadd, L. Tran, T. Vickers, J. Sindac, Z. V. Milanov, M. W. Holladay, S. S. Bhagwat, H. Hua, J. M. Ford Pulido, M. D. Cramer, D. Gitnick, J. James, A. Dao, B. Belli, R. C. Armstrong, D. K. Treiber and G. Liu, *Bioorg. Med. Chem. Lett.*, 2011, **21**, 5296-5300.
12. V. Bavetsias, A. Faisal, S. Crumpler, N. Brown, M. Kosmopoulou, A. Joshi, B. Atrash, Y. Perez-Fuertes, J. A. Schmitt, K. J. Boxall, R. Burke, C. Sun, S. Avery, K. Bush, A. Henley, F. I. Raynaud, P. Workman, R. Bayliss, S. Linardopoulos and J. Blagg, *J. Med. Chem.*, 2013, **56**, 9122-9135.
13. K. Strebhardt and A. Ullrich, *Nat. Rev. Cancer*, 2006, **6**, 321-330.
14. V. Archambault and D. M. Glover, *Nat. Rev. Mol. Cell Biol.*, 2009, **10**, 265-275.
15. R. E. Sherman, J. Li, S. Shapley, M. Robb and J. Woodcock, *N. Engl. J. Med.*, 2013, **369**, 1877-1880.
16. S. M. Lens, E. E. Voest and R. H. Medema, *Nat. Rev. Cancer*, 2010, **10**, 825-841.
17. J. J. Tyson, *Proc. Natl. Acad. Sci. U. S. A.*, 1991, **88**, 7328-7332.
18. B. Novak and J. J. Tyson, *J. Cell Sci.*, 1993, **106 (Pt 4)**, 1153-1168.
19. B. Novak and J. J. Tyson, *Proc. Natl. Acad. Sci. U. S. A.*, 1997, **94**, 9147-9152.
20. B. Novak, J. J. Tyson, B. Gyorffy and A. Csikasz-Nagy, *Nat. Cell Biol.*, 2007, **9**, 724-728.
21. J. R. Pomerening, E. D. Sontag and J. E. Ferrell, Jr., *Nat. Cell Biol.*, 2003, **5**, 346-351.
22. J. R. Pomerening, S. Y. Kim and J. E. Ferrell, Jr., *Cell*, 2005, **122**, 565-578.
23. J. E. Ferrell, Jr., T. Y. Tsai and Q. Yang, *Cell*, 2011, **144**, 874-885.
24. Q. Yang and J. E. Ferrell, Jr., *Nat. Cell Biol.*, 2013, **15**, 519-525.
25. J. B. Chang and J. E. Ferrell, Jr., *Nature*, 2013, **500**, 603-607.
26. A. Ciliberto and J. V. Shah, *EMBO J.*, 2009, **28**, 2162-2173.
27. J. Zou, S. D. Luo, Y. Q. Wei and S. Y. Yang, *Mol. Biosyst.*, 2011, **7**, 169-179.

Molecular BioSystems Accepted Manuscript

28. A. Seki, J. A. Coppinger, C. Y. Jang, J. R. Yates and G. Fang, *Science*, 2008, **320**, 1655-1658.
29. E. H. Chan, A. Santamaria, H. H. Sillje and E. A. Nigg, *Chromosoma*, 2008, **117**, 457-469.
30. D. Cimini, *Biochim. Biophys. Acta*, 2008, **1786**, 32-40.
31. H. B. Mistry, D. E. MacCallum, R. C. Jackson, M. A. Chaplain and F. A. Davidson, *Proc. Natl. Acad. Sci. U. S. A.*, 2008, **105**, 20215-20220.
32. A. Musacchio and E. D. Salmon, *Nat. Rev. Mol. Cell Biol.*, 2007, **8**, 379-393.
33. B. Ibrahim, S. Diekmann, E. Schmitt and P. Dittrich, *PLoS ONE*, 2008, **3**, e1555.
34. B. Ibrahim, E. Schmitt, P. Dittrich and S. Diekmann, *Biosystems*, 2009, **95**, 35-50.
35. B. Ibrahim, P. Dittrich, S. Diekmann and E. Schmitt, *Biophys. Chem.*, 2008, **134**, 93-100.
36. M. Simonetta, R. Manzoni, R. Mosca, M. Mapelli, L. Massimiliano, M. Vink, B. Novak, A. Musacchio and A. Ciliberto, *PLoS Biol.*, 2009, **7**, e10.
37. A. Doncic, E. Ben-Jacob, S. Einav and N. Barkai, *PLoS ONE*, 2009, **4**, e6495.
38. J. Pan and R. H. Chen, *Genes Dev.*, 2004, **18**, 1439-1451.
39. J. Nilsson, M. Yekezare, J. Minshull and J. Pines, *Nat. Cell Biol.*, 2008, **10**, 1411-1420.
40. A. Musacchio and A. Ciliberto, *Nat. Struct. Mol. Biol.*, 2012, **19**, 1059-1061.
41. K. Uzunova, B. T. Dye, H. Schutz, R. Ladurner, G. Petzold, Y. Toyoda, M. A. Jarvis, N. G. Brown, I. Poser, M. Novatchkova, K. Mechtler, A. A. Hyman, H. Stark, B. A. Schulman and J. M. Peters, *Nat. Struct. Mol. Biol.*, 2012, **19**, 1116-1123.
42. O. Gavet and J. Pines, *Dev. Cell*, 2010, **18**, 533-543.
43. R. Honda, R. Korner and E. A. Nigg, *Mol. Biol. Cell*, 2003, **14**, 3325-3341.
44. Z. Dai and L. Lai, *Mol. Biosyst.*, 2014, **10**, 1385-1392.
45. M. A. Lampson and T. M. Kapoor, *Nat. Cell Biol.*, 2005, **7**, 93-98.
46. C. J. Morrow, A. Tighe, V. L. Johnson, M. I. Scott, C. Ditchfield and S. S. Taylor, *J. Cell Sci.*, 2005, **118**, 3639-3652.
47. T. Kidokoro, C. Tanikawa, Y. Furukawa, T. Katagiri, Y. Nakamura and K. Matsuda, *Oncogene*, 2008, **27**, 1562-1571.
48. Y. Okamoto, T. Ozaki, K. Miyazaki, M. Aoyama, M. Miyazaki and A. Nakagawara, *Cancer Res.*, 2003, **63**, 4167-4173.
49. J. H. van Ree, K. B. Jeganathan, L. Malureanu and J. M. van Deursen, *J. Cell Biol.*, 2010, **188**, 83-100.
50. F. Girdler, K. E. Gascoigne, P. A. Eyers, S. Hartmuth, C. Crafter, K. M. Foote, N. J. Keen and S. S. Taylor, *J. Cell Sci.*, 2006, **119**, 3664-3675.
51. B. B. Gadea and J. V. Ruderman, *Mol. Biol. Cell*, 2005, **16**, 1305-1318.
52. M. G. Manfredi, J. A. Ecsedy, K. A. Meetze, S. K. Balani, O. Burenkova, W. Chen, K. M. Galvin, K. M. Hoar, J. J. Huck, P. J. LeRoy, E. T. Ray, T. B. Sells, B. Stringer, S. G. Stroud, T. J. Vos, G. S. Weatherhead, D. R. Wysong, M. Zhang, J. B. Bolen and C. F. Claiborne, *Proc. Natl. Acad. Sci. U. S. A.*, 2007, **104**, 4106-4111.
53. H. Yang, T. Burke, J. Dempsey, B. Diaz, E. Collins, J. Toth, R. Beckmann and X. Ye, *FEBS Lett.*, 2005, **579**, 3385-3391.
54. J. B. Fitzgerald, B. Schoeberl, U. B. Nielsen and P. K. Sorger, *Nat. Chem. Biol.*, 2006, **2**, 458-466.
55. A. S. Azmi, Z. Wang, P. A. Philip, R. M. Mohammad and F. H. Sarkar, *Mol. Cancer Ther.*, 2010, **9**, 3137-3144.
56. P. J. Yeh, M. J. Hegreness, A. P. Aiden and R. Kishony, *Nat. Rev. Microbiol.*, 2009, **7**, 460-466.
57. T. C. Chou, *Pharmacol. Rev.*, 2006, **58**, 621-681.
58. P. Csermely, T. Korcsmaros, H. J. Kiss, G. London and R. Nussinov, *Pharmacol. Ther.*, 2013, **138**, 333-408.
59. H. Eydgahi, W. W. Chen, J. L. Muhlich, D. Vitkup, J. N. Tsitsiklis and P. K. Sorger, *Mol. Syst. Biol.*, 2013, **9**, 644.
60. T. Khazaei, A. McGuigan and R. Mahadevan, *Front Physiol*, 2012, **3**, 135.

Molecular BioSystems Accepted Manuscript